



**Planar optomagnonic cavities driven by surface spin waves**Petros Andreas Pantazopoulos  and Nikolaos Stefanou *Section of Condensed Matter Physics, National and Kapodistrian University of Athens, Panepistimioupolis, GR-157 84 Athens, Greece*

(Received 7 January 2020; revised manuscript received 24 March 2020; accepted 27 March 2020; published 22 April 2020)

A generalized rigorous Floquet scattering-matrix method for stratified anisotropic optical media, subject to a periodic spatiotemporal modulation, is formulated and implemented. The method is applied for studying an optomagnonic cavity formed by an in-plane magnetized ferrite film, in which a magnetostatic surface spin wave propagates, sandwiched between two nonmagnetic dielectric Bragg mirrors. Our results provide unambiguous evidence that externally incident light, when trapped in a cavity mode, experiences a strongly enhanced interaction with the spin wave due to the increased coupling time, which can give rise to pronounced effects if the appropriate selection rules are fulfilled. By means of systematic calculations we reveal and explain some remarkable features of this interaction, such as formation of spectral gaps, controllable transmission, and the emergence of inelastic diffracted beams, and show that efficient conversion of the optical wave can be achieved by triply resonant inelastic scattering through (multi)magnon absorption and emission processes.

DOI: [10.1103/PhysRevB.101.134426](https://doi.org/10.1103/PhysRevB.101.134426)**I. INTRODUCTION**

The interaction of visible and near-infrared light with magnetostatic surface, so-called Damon-Eshbach [1], spin waves has long been investigated within different contexts. Brillouin light scattering, either by thermal incoherent magnetic excitations [2,3] or by externally excited coherent magnons [4–6], has been proven to be a powerful tool for the direct detection of Damon-Eshbach spin waves in magnetic thin films. In another perspective, epitaxially grown yttrium iron garnet (YIG) films on gadolinium gallium garnet substrates have been thoroughly studied both theoretically and experimentally [7–11] as high-frequency modulators for optical signal processing, employing Damon-Eshbach spin waves generated, e.g., by a microstrip line to diffract guided optical beams propagating in the same infrared-transparent YIG film. Further, significant effort has been devoted to improving the device performance using other ferrite materials with higher magneto-optic coupling constants [12–14] and/or designing multilayer configurations that comprise pairs of magnetic films [15–18]. For the same purpose, diffraction of guided light by other types of magnetostatic spin waves, such as forward-volume [9,19–21], backward-volume [12], and multiple-character [22] modes, as well as nonlinear magnetostatic surface waves [23] has been investigated, while nonuniform bias magnetic fields have also been applied [24,25] in order to enhance the diffraction and conversion efficiency.

More recently, there is growing interest in dual cavities for both light and spin waves, so-called optomagnonic, that would allow for an efficient coherent and reversible conversion between microwave and optical photons, mediated by magnons. This possibility would offer, among other things, a route for interfacing superconducting quantum circuits, which operate in the microwave frequency range, with optical and telecom photons in view of quantum information processing and communication applications [26,27]. In a broader perspective,

optomagnonic cavities provide a promising avenue for the realization of strong photon-magnon interaction phenomena, analogous to and even stronger than corresponding photon-phonon coupling effects in cavity optomechanics, allowing for coherent manipulation of elementary magnetic excitations in solids by optical means and vice versa [28–31].

Submillimeter-sized polished YIG spheres, hosting high-quality-factor and densely spaced optical whispering gallery modes (WGMs) in the near-infrared part of the spectrum and spin waves at gigahertz frequencies, can operate as optomagnonic cavities. Inelastic light scattering by the uniform-precession magnetic excitation in such cavities in the triple-resonance regime, in which the magnon provides the required energy and angular momentum for parity-conserving photon transitions from an initial to a final WGM, was observed [32–34] and analyzed [35]. However, the optomagnonic coupling was quite weak, and the attained optical-to-optical conversion efficiencies did not exceed  $10^{-5}$ . Significant experimental and theoretical effort was subsequently focused on improving the conversion efficiency by enhancing the mode overlap using higher-order Walker magnetostatic modes with nontrivial spin textures [36–38] or surface magnons of mixed dipolar-exchange character [39] interacting with optical WGMs in submillimeter-sized YIG spheres. Alternative proposals to enhance the optomagnonic interaction by reducing the modal volume, either employing Zeeman-split optical Mie resonances interacting with the uniform-precession spin wave in a magnetic garnet microsphere [40] or optical WGMs coupled through spin excitations localized at a magnetic vortex in a YIG microdisk [41], were suggested as well.

Meanwhile, planar optomagnonic architectures were also explored. Strong-coupling effects beyond the linear-response approximation, which can lead to enhanced modulation of externally incident light by perpendicular spin waves through multimagnon emission and absorption processes, were anticipated in a multilayer structure comprising a magnetic film

between two nonmagnetic dielectric Bragg mirrors [42] as well as in an all-magnetic dielectric one-dimensional dual photonic-magnonic crystal with a localized defect [43], using an adiabatic quasistatic method. However, in the spirit of the adiabatic approximation, the frequency of the optical field remains unchanged, and thus, triply resonant inelastic scattering cannot be accounted for by this approach. A rigorous, fully dynamic time-Floquet scattering-matrix method for the accurate description of stratified optomagnonic structures that remain invariant parallel to the interfaces under the action of the spin wave was subsequently developed [44]. Application of this method to an in-plane magnetized ferrite film sandwiched between two lossless dielectric Bragg mirrors revealed the occurrence of strong triply resonant inelastic light scattering by the uniform-precession mode, with high magnon-mediated optical-to-optical conversion efficiencies reaching 30% [45]. A high-efficiency microwave-to-optical-photon converter for quantum information processing and communication applications, based on the diffraction of guided light by a traveling Damon-Eshbach spin wave in a design similar to that of magneto-optical modulators, was also proposed [46]. However, a rigorous computational method for general planar optomagnonic structures in the presence of spin waves that induce, in addition to the temporal modulation, an in-plane periodic spatial corrugation, such as the magnetostatic surface and volume spin waves, is still lacking.

The present paper is meant to provide a comprehensive theoretical study of the interaction of externally incident light with Damon-Eshbach spin waves in a versatile planar optomagnonic cavity, formed by a magnetic garnet film between two lossless dielectric Bragg mirrors, using a generalization of our recently developed time-Floquet scattering-matrix method to stratified photonic media driven by a spatiotemporal periodic stimulus. Some parts of the formalism presented here cannot be deduced in a straightforward manner from our previous method and require particular care. That is why we deferred the derivation of those parts to the Appendix while, for the rest of the method, the reader is referred to Ref. [44]. The fully dynamic spatiotemporal Floquet scattering-matrix methodology reported here represents a considerable advance over our previous work and could be useful, also, for studying the more general class of driven Floquet space-time crystals and metamaterials, which have received increasing attention in recent years [47–50]. The remainder of the paper is organized as follows. In Sec. II we discuss the optical response of our statically magnetized structure. In Sec. III we briefly summarize the theory of magnetostatic surface spin waves and deduce the selection rules that govern the optomagnonic interaction in the case under consideration. Section IV is devoted to the presentation and interpretation of our numerical results for the inelastic light–spin-wave scattering, while the last section concludes the paper.

## II. STATICALLY MAGNETIZED STRUCTURE

In order to achieve simultaneous confinement of light and spin waves in the same region of space, we consider the same planar structure as that studied in Ref. [45]. It consists of a cerium-substituted yttrium iron garnet (Ce:YIG) film sandwiched between two lossless Bragg mirrors, each composed

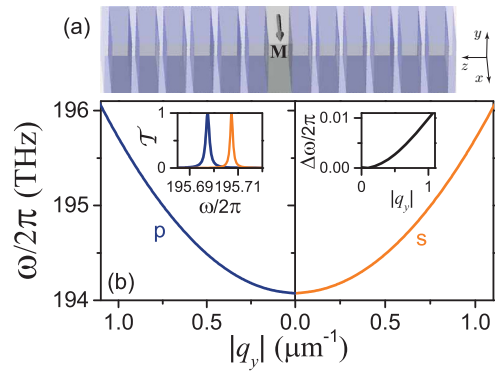


FIG. 1. (a) Schematic view of a symmetric planar optomagnonic cavity, realized by a 340-nm-thick, in-plane magnetized Ce:YIG film, sandwiched between two Bragg mirrors. Each Bragg mirror consists of six periods of alternating Si and SiO<sub>2</sub> layers with a thickness of 110 and 265 nm, respectively. (b) Dispersion curves of the p- and s-polarized resonant defect modes,  $\omega_p(q_y)$  and  $\omega_s(q_y)$ , within the lowest Bragg gap. The left inset depicts the corresponding transmission resonances for light incident from the left with  $|q_y| = 1 \mu\text{m}^{-1}$ , neglecting material losses. The frequency difference of the p and s modes at the same  $q_y$  is shown in the right inset.

of six periods of alternating Si and SiO<sub>2</sub> layers, as schematically depicted in Fig. 1(a). The structure is grown along the  $z$  direction from left to right and is embedded in air. We consider the Voigt geometry; that is, the Ce:YIG film is magnetically saturated to  $M_0$  by an in-plane bias field  $H_0$  along the  $x$  direction, and light propagates perpendicular to it (in the  $y$ - $z$  plane). We choose an in-plane component of the wave vector  $q_y = 1 \mu\text{m}^{-1}$  and an operation wavelength  $\lambda \simeq 1.55 \mu\text{m}$ . Si and SiO<sub>2</sub> are optically isotropic materials and lossless at the given wavelength ( $n_{\text{Si}} = 3.5$ ,  $n_{\text{SiO}_2} = 1.47$ ), at which Ce:YIG is characterized by a relative electric permittivity tensor,

$$\epsilon = \begin{pmatrix} \epsilon & 0 & 0 \\ 0 & \epsilon & if \\ 0 & -if & \epsilon \end{pmatrix}, \quad (1)$$

with  $\epsilon = 5.10 + i5 \times 10^{-5}$  and  $f = -0.008$  [51–53]. The thickness of the layers is determined following the structure-design strategy proposed in Ref. [45]: The quarter-wavelength condition yields 110- and 265-nm-thick Si and SiO<sub>2</sub> layers, respectively, while the half-wavelength Ce:YIG film has a thickness  $d = 340$  nm. We note that the relative magnetic permeability of the materials equals unity.

The structure is illuminated from the left with linearly polarized light of angular frequency  $\omega$  and in-plane wave-vector component  $q_y$ . In the chosen configuration, linearly polarized light with its electric field oscillating in and normal to the plane of incidence, termed p and s polarized, respectively, is an eigenmode of the system [45]. Due to the presence of the magnetic film, which can be considered a defect in the periodic sequence of layers of the Bragg mirrors, the structure supports resonant defect modes within the lowest Bragg gap manifested as sharp peaks in the corresponding transmission spectrum. Figure 1(b) shows the dispersion curves of these modes,  $\omega_p(q_y)$  and  $\omega_s(q_y)$ , as a function of  $|q_y|$  because the eigenfrequencies depend on the magnitude but not on the

sign of  $q_y$  since the structure remains invariant under the combined operations of rotation through an angle  $\pi$  about the  $y$  axis followed by time reversal, which transforms  $(q_y, q_z)$  to  $(-q_y, q_z)$ . At any angle of incidence,  $\theta = \sin^{-1}(cq_y/\omega)$ , with  $c$  being the speed of light in vacuum, the structure exhibits two high-quality-factor defect resonances (one for each polarization), with their frequency difference being of the order of 10 GHz, as shown in the right inset of Fig. 1(b), which matches the frequency of magnetostatic surface spin waves (see the next section). The structure is fully transparent at each of those resonances if material losses are neglected, as shown, for instance, in the left inset of Fig. 1(b) for  $\theta \simeq 14^\circ$  ( $q_y = 1 \mu\text{m}^{-1}$ ).

When dissipative losses are taken into account, the position of the resonances remains practically unchanged, but their quality factor and, consequently, the transmission peaks are significantly reduced. For example, for  $q_y = 1 \mu\text{m}^{-1}$ , the transmission at the p (s) resonance drops from 100% to 45% (35%), while 44% (48%) of the incident light intensity is absorbed. Nevertheless, the resonances remain well resolved.

### III. OPTICAL-SPIN WAVE INTERACTION

The Ce:YIG film described in the previous section supports magnetostatic surface spin waves that propagate with wave number  $Q$  along the  $y$  direction. Their angular frequency  $\Omega$  obeys the dispersion relation [54]

$$\Omega^2 = \Omega_H(\Omega_H + \Omega_M) + \frac{\Omega_M^2}{4}[1 - \exp(-2Qd)], \quad (2)$$

with  $\Omega_H = \gamma\mu_0 H_0$  and  $\Omega_M = \gamma\mu_0 M_0$ , where  $\gamma$  is the gyromagnetic ratio and  $\mu_0$  is the magnetic permeability of vacuum. The dynamic magnetization field, which has the form of a monochromatic harmonic wave, is related through the Polder susceptibility tensor to the associated magnetic field. The latter is derived from a magnetostatic potential that satisfies Walker's equation, subject to the appropriate boundary conditions [54]. It comes out that, for each value of  $Q$ , there are two modes of the same frequency, which propagate in the positive ( $S = +$ ) and negative ( $S = -$ )  $y$  directions, with the corresponding magnetization field given by

$$\begin{aligned} \mathbf{M}(\mathbf{r}, t)/M_0 = & \widehat{\mathbf{x}} + \eta_{Sy}(z)\sin(SQy - \Omega t)\widehat{\mathbf{y}} \\ & + \eta_{Sz}(z)\cos(SQy - \Omega t)\widehat{\mathbf{z}}, \end{aligned} \quad (3)$$

where

$$\begin{aligned} \eta_{Sy}(z) = & \eta_0\{(S\chi + \kappa)\exp(-Qz) \\ & + S(\chi + 2 + S\kappa)\exp[Q(d + z)]\}, \\ \eta_{Sz}(z) = & \eta_0\{(\chi + S\kappa)\exp(-Qz) \\ & - (\chi + 2 + S\kappa)\exp[Q(d + z)]\}, \end{aligned} \quad (4)$$

with  $\chi = \Omega_H\Omega_M/(\Omega_H^2 - \Omega^2)$  and  $\kappa = \Omega\Omega_M/(\Omega_H^2 - \Omega^2)$  being the elements of the Polder susceptibility tensor and  $\eta_0$  being an arbitrary amplitude factor that must be chosen such that the magnetization precession angle does not exceed a few degrees in order to ensure that we are in the linear regime. The magnetization profile given by Eq. (3) shifts from one side of the film at  $z = -d/2$  to the other at  $z = d/2$  when the propagation direction is reversed, which is a manifestation of

nonreciprocity of the Damon-Eshbach spin waves. For typical values of the bias field and the saturation magnetization,  $H_0 = 2.6 \text{ kOe}$  and  $M_0 = 150 \text{ kA/m}$  [51],  $\Omega/2\pi$  is of the order of 10 GHz. We note that exchange fields, quantified by the exchange stiffness constant  $\alpha_{\text{ex}}$ , may also be important for the description of spin waves. However, in our case here ( $\alpha_{\text{ex}} \sim 3 \times 10^{-16} \text{ m}^2$ ) [54], for  $Q$  of the order of  $1 \mu\text{m}^{-1}$  or less, their contribution can be ignored since  $\alpha_{\text{ex}}Q^2 < 10^{-3}$  and  $\alpha_{\text{ex}}\pi^2/d^2 \sim 10^{-2}$  [55,56]. Therefore, the exchange-free description of Damon-Eshbach spin waves is appropriate, except perhaps for narrow special regions due to the interaction of surface and volume modes [55].

The interaction between light and magnetostatic surface spin waves enters through the electric permittivity tensor. Specifically, the magnetization field given by Eq. (3) induces a spatiotemporal perturbation [42]

$$\begin{aligned} \delta\epsilon(y, z, t) = & \frac{1}{2}\{\delta\epsilon(z)\exp[i(SQy - \Omega t)] \\ & + \delta\epsilon^\dagger(z)\exp[-i(SQy - \Omega t)]\} \end{aligned} \quad (5)$$

in the electric permittivity tensor of the statically magnetized material, where

$$\delta\epsilon(z) = f \begin{pmatrix} 0 & i\eta_{Sz}(z) & -\eta_{Sy}(z) \\ -i\eta_{Sz}(z) & 0 & 0 \\ \eta_{Sy}(z) & 0 & 0 \end{pmatrix} \quad (6)$$

and the dagger denotes Hermitian conjugation.

The selection rules that govern the optomagnonic interaction can be deduced from the expression of the coupling strength associated with the photon-magnon scattering. To first-order Born approximation, this is proportional to the overlap integral  $G = \langle f | \delta\epsilon | i \rangle$ , where  $\langle \alpha \mathbf{r}' t' | i \rangle = E_{i\alpha}(z)\exp[i(q_{ix}x + q_{iy}y - \omega_i t)]$  and  $\langle f | \alpha \mathbf{r} t \rangle = E_{f\alpha}^*(z)\exp[-i(q_{fx}x + q_{fy}y - \omega_f t)]$  denote Cartesian components ( $\alpha = x, y, z$ ) of the incoming and outgoing monochromatic time-harmonic fields in the static magnetic structure. Using Eq. (5), we obtain

$$\begin{aligned} G = & \delta(q_{ix} - q_{fx})[\delta(q_{iy} - q_{fy} - SQ)\delta(\omega_i - \omega_f - \Omega)g_- \\ & + \delta(q_{iy} - q_{fy} + SQ)\delta(\omega_i - \omega_f + \Omega)g_+], \end{aligned} \quad (7)$$

where

$$\begin{aligned} g_+ = & i\frac{4\pi^3 f}{M_0} \int dz \mathbf{m}(z) \cdot [\mathbf{E}_f^*(z) \times \mathbf{E}_i(z)], \\ g_- = & i\frac{4\pi^3 f}{M_0} \int dz \mathbf{m}^*(z) \cdot [\mathbf{E}_f^*(z) \times \mathbf{E}_i(z)], \end{aligned} \quad (8)$$

with  $\mathbf{m}(z) = M_0[i\eta_{Sy}(z)\widehat{\mathbf{y}} + \eta_{Sz}(z)\widehat{\mathbf{z}}]$ . The delta functions in Eqs. (7) express conservation of in-plane momentum and energy in inelastic light scattering processes that involve emission and absorption of one magnon by a photon, as expected in the linear regime. Equations (8) provide the necessary selection rules that govern the optomagnonic interaction. When the polarization vectors of  $\mathbf{E}_i$  and  $\mathbf{E}_f$  are real, as in the case of linear polarization considered here, nonvanishing optomagnonic coupling is obtained for EM fields of orthogonal polarizations.

Conservation of in-plane momentum and energy and polarization conversion for one-magnon processes imply that, e.g., s-polarized incident light with in-plane wave-vector component  $q_{iy}$  and angular frequency  $\omega_i$ , through inelastic scattering

by absorption or emission of  $n$  magnons, will be converted to a final state with in-plane wave-vector component  $q_{fy} = q_{iy} - n\Omega(Q)$ , angular frequency  $\omega_f = \omega_i - n\Omega(Q)$ , and appropriate polarization. We recall that the polarization of the photon changes (remains the same) upon absorption or emission of an odd (even) number of magnons  $n$ . Obviously, efficient conversion occurs when resonant initial and final optical modes are involved. For instance, for s-polarized light incident with given  $\{q_{iy}, \omega_i\}$  within the width of the corresponding defect resonance at  $\omega_s(q_{iy})$  [see Fig. 1(b)], strong inelastic scattering is expected when, upon absorption or emission of magnons with  $\{Q, \Omega(Q)\}$ , the conservation rules lead to a final photon state at an appropriate defect resonance of the statically magnetized structure [see Fig. 1(b)], with the triple-resonance condition achieved exactly for  $\omega_i = \omega_s(q_{iy})$ . Otherwise, the dynamic structure behaves as if it were static. These expectations are, indeed, verified by our results presented in the subsequent section. We note that nonreciprocity of the Damon-Eshbach spin wave is accounted for by the selection rules and the magnetization profile through  $S$ , which changes sign upon reversing the propagation direction.

#### IV. SPATIOTEMPORAL OPTOMAGNONIC STRUCTURE

The structure considered in the present study is the same as the one in our previous work [45]; however, the system is completely different because, here, the cavity is driven by a Damon-Eshbach spin wave, which induces a spatiotemporal and not simply a temporal modulation. This gives rise to some remarkable peculiar effects, such as the formation of spectral gaps and controllable transmission through triply resonant inelastic diffraction, that will be analyzed below.

Let us assume continuous excitation of a magnetostatic surface spin wave of wave number  $Q$  and frequency  $\Omega(Q)$  propagating in the positive  $y$  direction, noting that such a mode can be excited more efficiently [9]. We take  $\Omega_H = 1.4\Omega_M$ , which yields  $\Omega$  of the order of 10 GHz. We further assume an appropriate amplitude factor  $\eta_0$  of the magnetization field for every chosen value of  $Q$  corresponding to a maximum cone angle of the (elliptical) magnetization precession of  $7^\circ$ . The structure is illuminated from the left by s-polarized light with  $q_{iy} = 1 \mu\text{m}^{-1}$  and angular frequency  $\omega_i$  within the width of the corresponding defect resonance at  $\omega_s(q_{iy})$ , depicted in Fig. 1(b). The dynamic optical response of the structure is calculated using an extension of our recently developed time-Floquet scattering-matrix method [44] to stratified media driven by a spatiotemporal periodic stimulus, which is summarized in the Appendix. Considering a cutoff of  $N = 10$  in the Fourier series expansions involved and discretizing the magnetic film into 40 elementary sublayers ensure excellent convergence of our numerical results. To begin with, we neglect materials' losses in order to better highlight the effects.

Figure 2 displays the elastic transmittance [Figs. 2(a) and 2(d)] and reflectance [Figs. 2(b) and 2(e)] as a function of the wave number of the spin wave and the detuning of the input optical frequency from the s defect resonance (at the given  $q_{iy} = 1 \mu\text{m}^{-1}$ ) in regions about the lines  $\omega_i = \omega_p(q_{iy} - nQ) + n\Omega(Q)$ , where  $p = p$  or  $s$  for odd or even values of  $n$ , respectively. These lines express the appropriate conservation rules for photon transitions to a defect resonance (dashed

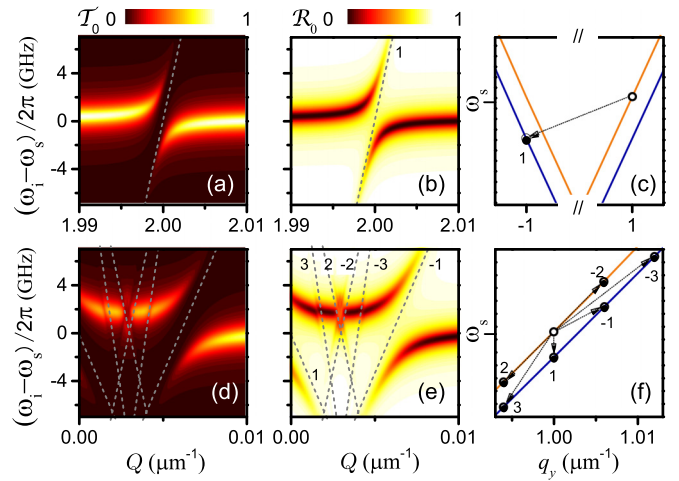


FIG. 2. The structure of Fig. 1(a), subject to continuous excitation of a magnetostatic surface spin wave of wave number  $Q$  propagating along the positive  $y$  direction, is illuminated from the left by s-polarized light with  $q_{iy} = 1 \mu\text{m}^{-1}$  and angular frequency  $\omega_i$  within a short range about the corresponding defect resonance at  $\omega_s = \omega_s(q_{iy})$  [see Fig. 1(b)]. Material losses are neglected. For the spin wave we assume  $\Omega_H = 1.4\Omega_M$  and an amplitude factor  $\eta_0$  corresponding to a maximum cone angle of the (elliptical) magnetization precession of  $7^\circ$  for each value of  $Q$ . Variation of (a) and (d) the elastic transmission and (b) and (e) reflection spectra in the vicinity of triply resonant optical transitions. The dashed lines express the conservation rules for converting the input light to the appropriate (p or s) final resonant state through  $n$ -magnon absorption ( $n < 0$ ) or emission ( $n > 0$ ), denoted by the numbers in (b) and (e). (c) and (f) Illustration of the corresponding triply resonant processes, where open and solid circles refer to the initial and final states, respectively.

lines in Fig. 2), which are fulfilled either for  $Q \simeq 2 \mu\text{m}^{-1}$  or for  $Q < 0.01 \mu\text{m}^{-1}$ , as shown in the top and bottom panels of Fig. 2. It is in the proximity of these lines that the optical response of the structure is significantly affected by the spin waves. Specifically, the elastic transmission is drastically suppressed, while the elastic reflection is increased. However, their sum does not equal unity, which indicates an energy transfer from the elastic to the inelastic outgoing beams. Remarkably, at the triple-resonance condition, the elastic transmission practically vanishes. Figures 2(c) and 2(f) depict the initial and final optical modes of the statically magnetized structure for which the triple-resonance condition is met through  $n$ -magnon absorption ( $n < 0$ ) and emission ( $n > 0$ ) processes with  $|n| \leq 3$ . It is worth noting that the triple-resonance condition is met also for  $nQ = 2 \mu\text{m}^{-1}$ ,  $n = 2, 3$ , but the effect is considerably weaker. We also note that the elastic transmitted and reflected beams are predominantly s polarized.

Let us further analyze the one-magnon emission processes ( $n = 1$ ) for  $Q \simeq 2 \mu\text{m}^{-1}$ , evident in the top panel of Fig. 2. As expected from Figs. 2(a) and 2(b), the total elastic outgoing beam intensity,  $\mathcal{I}_0 = \mathcal{T}_0 + \mathcal{R}_0$ , shown in Fig. 3(a), is reduced only in the vicinity of  $Q$  and  $\omega_i$  for which the conservation rules are met. That is where the total inelastic  $n = 1$  beam intensity  $\mathcal{I}_1$  is increased, as illustrated in Fig. 3(b). In other words, energy is transferred from the  $n = 0$  to the  $n = 1$

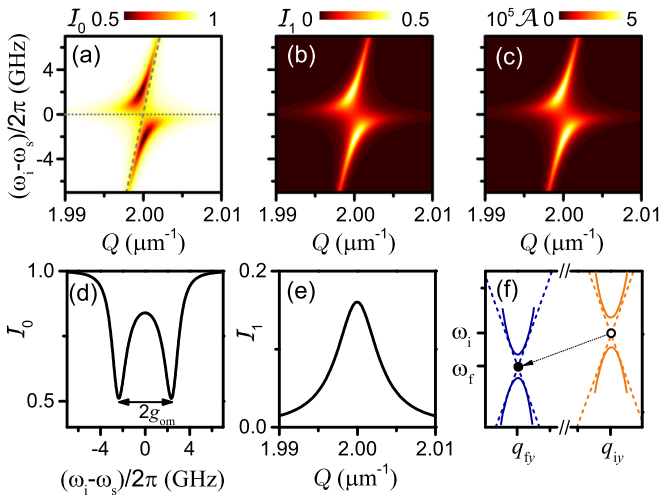


FIG. 3. The structure of Fig. 1(a), subject to continuous excitation of a magnetostatic surface spin wave of wave number  $Q$  propagating along the positive  $y$  direction, is illuminated from the left by  $s$ -polarized light with  $q_{iy} = 1 \mu\text{m}^{-1}$  and angular frequency  $\omega_i$  within a short range about the corresponding defect resonance at  $\omega_s = \omega_s(q_{iy})$  [see Fig. 1(b)]. Material losses are neglected. For the spin wave we consider  $\Omega_H = 1.4\Omega_M$  and an amplitude factor  $\eta_0 = 0.015$ . Variation of (a) the total elastic ( $n = 0$ ) and (b)  $n = 1$  inelastic outgoing light beam intensities,  $\mathcal{I}_0$  and  $\mathcal{I}_1$ , respectively, in the vicinity of triply resonant optical transitions. The dashed line expresses the conservation rules for converting the input light to a  $p$  final resonant state through one-magnon emission ( $n = 1$ ):  $\omega_i = \omega_p(q_{iy} - Q) + \Omega(Q)$ . The dotted line corresponds to  $\omega_i = \omega_s$ . (c) Corresponding variation of the total optical absorption. (d) Variation of  $\mathcal{I}_0$  versus the detuning of the incident light frequency at  $Q = 2 \mu\text{m}^{-1}$ , for which  $\Omega = \omega_s - \omega_p(q_{iy} - Q)$ . From this diagram, the optomagnonic coupling strength  $g_{om}$  can be readily deduced. (e) Variation of  $\mathcal{I}_1$  versus  $Q$  for  $\omega_i = \omega_s$ . (f) Schematic illustration of the opening of the Bragg gap due to the excitation of spin waves with wave number  $Q = q_{iy} - q_{iy}$ .

outgoing light beam.  $\mathcal{I}_1$  is predominantly  $p$  polarized and almost equally distributed between the corresponding transmitted and reflected beams.

Interestingly, right at the triple-resonance condition, inelastic light scattering is not maximized; on the contrary, it is greatly reduced. This apparently counterintuitive feature can be understood as follows. Enhanced inelastic scattering of light occurs when the wave number  $Q$  and corresponding angular frequency  $\Omega(Q)$  of a magnon match a photon transition between two resonant modes (triple-resonance condition). In this respect, based on the results for the statically magnetized structure, depicted in Fig. 1(b), for an optical defect resonance at  $\omega_s(q_{iy})$ , say, with  $q_{iy} > 0$ , excited by  $s$ -polarized light incident with the given  $q_{iy}$ , one would expect considerable intensity in the outgoing beam of photons that emitted one magnon ( $n = 1$ ) if the final photon state is at a  $p$ -polarized resonance with  $\omega_p(q_{fy}) = \omega_s(q_{iy}) - \Omega(Q)$  and  $q_{fy} = q_{iy} - Q$ . However, this picture is not quite correct. The spin wave induces a (dynamic) corrugation in the  $y$  direction, with period  $\Lambda = 2\pi/Q$ , which leads to the opening of Bragg gaps at  $q_y = Q/2$ , i.e., at  $q_y = (q_{iy} - q_{fy})/2 \simeq q_{iy}$  in our case, since  $q_{fy} \simeq q_{iy}$ . Therefore, in the driven system, there

appear two defect resonant modes at  $q_{iy}$ , which are relatively largely shifted downwards and upwards in frequency from the respective original optical resonance at  $\omega_s(q_{iy})$ , as schematically depicted in Fig. 3(f). As a result, in the vicinity of  $Q$ , as estimated from the statically magnetized structure, we obtain strong inelastic light scattering in the bright regions of Fig. 3(b) that satisfy the triple-resonance condition at frequencies considerably redshifted and blueshifted away from  $\omega_s(q_{iy})$ . For larger or smaller values of  $Q$ , the Bragg gaps open up at higher or lower frequencies, respectively, and thus, the optical resonance of the statically magnetized structure at  $\omega_s(q_{iy})$  is less affected. Therefore, these bright areas tend to approach that frequency, although they quickly disappear as  $Q$  increases or decreases further because the triple-resonance condition can no longer be satisfied. The strong inelastic light scattering depicted in Fig. 3(b), which can be as large as 50%, is accompanied by an excess number of magnons emitted, which can be accounted for by our fully spatiotemporal Floquet scattering-matrix method. This is manifested as increased optical absorption in the bright regions in Fig. 3(c).

From the variation of  $\mathcal{I}_0$  versus the detuning of the incident light frequency, at  $Q = 2 \mu\text{m}^{-1}$ , for which  $\Omega = \omega_s - \omega_p(q_{iy} - Q)$ , one can estimate the optomagnonic coupling strength  $g_{om}$  [57]. From Fig. 3(d), we extract  $g_{om} = 2.3$  GHz, which is comparable to the width of the optical resonance(s), indicating that we are in the strong-coupling regime. On the other hand, for  $\omega_i = \omega_s(q_{iy})$ , although the Bragg gap is clearly manifested in the variation of  $\mathcal{I}_1$  at  $Q = 2 \mu\text{m}^{-1}$  (triple-resonance condition), the intensity of the  $n = 1$  inelastic outgoing beam exhibits a maximum reaching 15%, as shown in Fig. 3(e), because of the finite lifetime of the modes in the vicinity of the Bragg gap. This feature indicates, along with the fact that the elastic transmission vanishes, that only the converted  $p$ -polarized light with frequency  $\omega_s - \Omega$  is transmitted through the structure at an angle of about  $-14^\circ$ .

We shall now focus on the region  $Q < 0.1 \mu\text{m}^{-1}$  shown in the bottom panel of Fig. 1. In this case, the conservation rules are accomplished for up to  $n = 10$ ; however, the most prominent effects occur for  $|n| \leq 3$ . Figure 4 displays the variation of the total elastic and inelastic outgoing light beam intensities  $\mathcal{I}_n$  for  $|n| \leq 3$  versus the detuning of the input frequency from the  $s$  defect resonance and the wave number of the spin wave, along with the corresponding variation of the total optical absorption. As before,  $s$ -polarized light impinges on the structure from the left with  $q_{iy} = 1 \mu\text{m}^{-1}$  and angular frequency  $\omega_i$ . It can be seen that, again, when the appropriate conservation conditions are met for given  $n$ , energy is transferred from the elastic to the corresponding inelastic beam, resulting in bright areas in the relevant diagrams. Right at the triple-resonance conditions, Bragg gaps open up, although their fingerprints are not clearly discernible in the diagrams for  $n = \pm 2, \pm 3$ . Depending on the process, i.e., magnon emission (absorption), there is a net energy transfer from (to) the photon to (from) the magnon field, yielding optical loss (gain) in the absorption spectrum displayed in Fig. 4(e). We note that, here, the total inelastic outgoing light intensity is almost equally distributed between the transmitted and reflected beams and is predominantly  $p$  ( $s$ ) polarized for odd (even)  $n$ . Remarkably, except for the high magnon-mediated

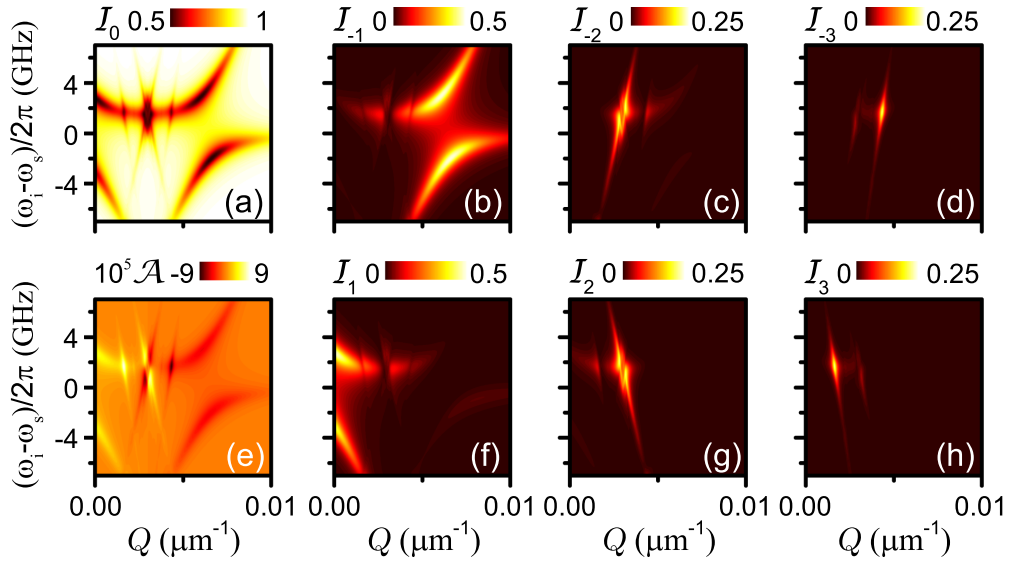


FIG. 4. The structure of Fig. 1(a), subject to continuous excitation of a magnetostatic surface spin wave of wave number  $Q$  propagating along the positive  $y$  direction, is illuminated from the left by s-polarized light with  $q_{iy} = 1 \mu\text{m}^{-1}$  and angular frequency  $\omega_i$  within a short range about the corresponding defect resonance at  $\omega_s = \omega_s(q_{iy})$  [see Fig. 1(b)]. Material losses are neglected. For the spin wave we consider  $\Omega_H = 1.4\Omega_M$  and an amplitude factor  $\eta_0 = 0.04$ . (a)–(d) and (f)–(h) Variation of the total elastic and inelastic outgoing light beam intensities  $\mathcal{I}_n$ ,  $|n| \leq 3$ , in the vicinity of triply resonant optical transitions and (e) the corresponding variation of the optical absorption.

optical-to-optical conversion efficiency, reaching 50% for the one-magnon ( $n = \pm 1$ ) processes, high conversion efficiency, up to 25%, is attained for absorption and emission of two or three magnons by a photon. In other words, the optical response of the structure is strongly modulated through the excitation of the spin waves. In the particular case of incident light at the s defect resonance, when the triple-resonance condition is met, e.g., for  $n = \pm 1$ , the elastic transmission practically vanishes. Most of the outgoing light is directed to the elastic reflection channel, and the rest is almost equally distributed between the inelastic transmitted and reflected

beams. However, since  $Q \ll q_{iy}$ , the deflection of the inelastic outgoing beams is very small. We note in passing that the optomagnonic coupling strength for the one-magnon absorption process here is 2.9 GHz, which is similar to that obtained in the one-magnon emission process for  $Q = 2 \mu\text{m}^{-1}$  discussed above.

When dissipative losses are taken into consideration, the static structure is no longer fully transparent at both s and p defect resonances. Moreover, while the main features of the diagrams associated with elastic and inelastic processes are not qualitatively altered (compare Figs. 4 and 5 for the

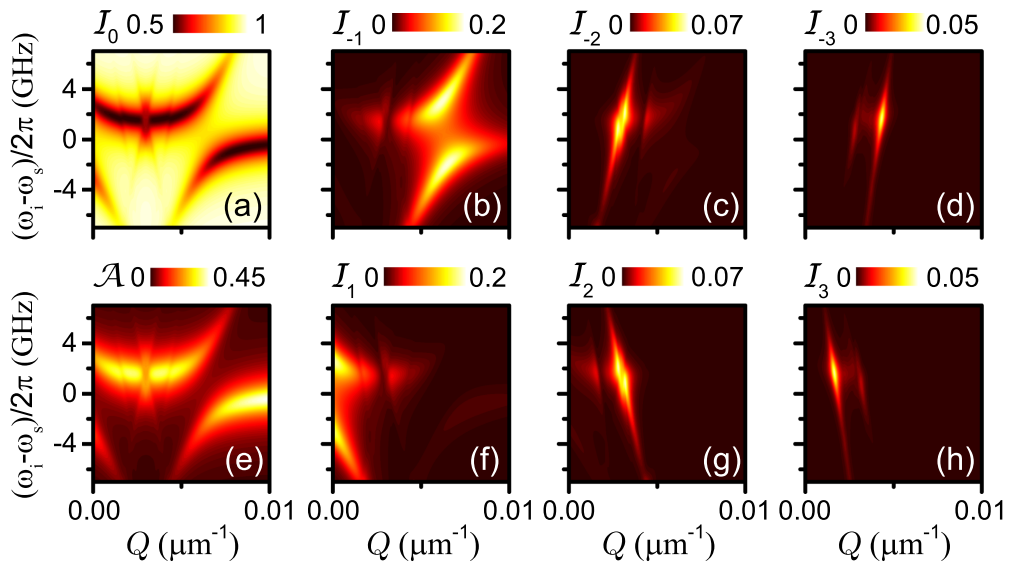


FIG. 5. The structure of Fig. 1(a), with realistic material losses, subject to continuous excitation of a magnetostatic surface spin wave of wave number  $Q$  propagating along the positive  $y$  direction, is illuminated from the left by s-polarized light with  $q_{iy} = 1 \mu\text{m}^{-1}$  and angular frequency  $\omega_i$  within a short range about the corresponding defect resonance at  $\omega_s = \omega_s(q_{iy})$  [see Fig. 1(b)]. For the spin wave we consider  $\Omega_H = 1.4\Omega_M$  and an amplitude factor  $\eta_0 = 0.04$ . (a)–(d) and (f)–(h) Variation of the total elastic and inelastic outgoing light beam intensities  $\mathcal{I}_n$ ,  $|n| \leq 3$ , in the vicinity of triply resonant optical transitions and (e) the corresponding variation of the optical absorption.

low- $Q$  region, but similar results are obtained for  $Q$  about  $2\ \mu\text{m}^{-1}$  as well), the elastic transmission and the inelastic outgoing light beam intensities are significantly lowered. In addition, material losses, now, dominate the absorption spectrum [compare Figs. 4(e) and 5(e)], except for the Bragg-gap regions where light is mostly reflected. Remarkably, the optomagnonic structure under study, even under realistic conditions, at the triple-resonance condition for  $n = \pm 1$  blocks the elastic transmission channel with the corresponding inelastic transmitted and reflected beam intensities being as high as 5%. Moreover, high optical-to-optical conversion efficiencies can also be obtained through multimagnon exchange processes. For example, at the triple-resonance condition, almost 6% and 2% of the incident light can be transmitted via two- and three-magnon absorption and/or emission processes, respectively. We also note that the dissipative losses do not significantly reduce the optomagnonic coupling strength, which, for the one-magnon processes, equals 2.2 and 2.8 GHz for large and small values of  $Q$ , respectively. As a final remark we mention that, by reducing the spin-wave amplitude, while Bragg gaps and multimagnon processes are gradually suppressed, one-magnon effects remain considerable.

## V. SUMMARY AND CONCLUSION

In summary, we reported a thorough investigation of the interaction of light with magnetostatic surface spin waves in a layered optomagnonic structure by means of rigorous calculations using an extension of our recently developed fully dynamic time-Floquet scattering-matrix method to stratified media subject to a periodic spatiotemporal modulation. In the design under consideration, concurrent localization of the interacting optical and magnetization fields is achieved in an in-plane magnetized Ce:YIG film which, placed between two lossless symmetric Si/SiO<sub>2</sub> Bragg mirrors, acts as a dual cavity for both photons and magnons. As a result, the interaction time greatly increases, and coupling strengths comparable to the width of the optical resonance(s) can be attained. Based on the optical response of the statically magnetized structure, we derived general conservation and selection rules that govern photon-to-photon conversion through absorption or emission of magnons. When these rules are fulfilled, our systematic calculations provide compelling evidence for the occurrence of remarkable and strong inelastic scattering effects, which subsist even in the presence of optical losses and enable efficient modulation of propagating light. Intriguing phenomena, such as formation of band gaps in the elastic and inelastic scattering spectra, emergence of inelastic diffracted beams, blocking of the elastic transmission channel, and (multi)magnon-mediated high optical-to-optical conversion efficiencies were analyzed, and a consistent interpretation of the underlying physics was provided. As a final note, we stress that the spatiotemporal Floquet scattering-matrix method developed here is directly applicable to planar optomagnonic structures driven by an arbitrary surface or volume spin wave and can be easily adapted to describe any kind of wave propagating in a stratified medium subject to a periodic spatiotemporal disturbance.

## ACKNOWLEDGMENTS

P.A.P. was supported by the General Secretariat for Research and Technology (GSRT) and the Hellenic Foundation for Research and Innovation (HFRI) through a Ph.D. scholarship (No. 906).

## APPENDIX: SPATIOTEMPORAL FLOQUET SCATTERING-MATRIX METHOD

The dynamic optical response of the structure under consideration, subject to continuous excitation of a magnetostatic surface spin wave, can be studied by properly extending the time-Floquet scattering-matrix method that we recently developed for periodically time-varying stratified photonic media [44]. In our case here, as dictated by Eq. (5), we have to deal with a structure in which the spin wave induces, in addition, a periodic spatial corrugation perpendicular to the direction of growth.

Let us consider a medium, characterized by a scalar relative magnetic permeability  $\mu$  and a relative electric permittivity tensor of the form  $\epsilon(\mathbf{r}, t) = \epsilon(y - S\frac{\Omega}{Q}t)$ , which varies periodically with a period  $\Lambda = 2\pi/Q$ , i.e.,  $\epsilon(\xi) = \epsilon(\xi + \Lambda)$ . Such a variation can be induced by a sinusoidal pump wave of wavelength  $\Lambda = 2\pi/Q$  and period  $T = 2\pi/\Omega$ . If the time variation of the permittivity is very slow compared to the period of an optical wave, assuming Floquet-type solutions of the form  $\mathbf{F}(\mathbf{r}, t) = \text{Re}\{\mathcal{F}(\mathbf{r}, t) \exp[i(q_y y - \omega t)]\}$  for the electric and magnetic fields ( $\mathbf{F} = \mathbf{E}, \mathbf{H}$ ), Maxwell equations read [44]

$$\begin{aligned} \nabla \times \mathcal{E}(\mathbf{r}, t) \exp[i(q_y y - \omega t)] \\ &= -\mu_0 \mu \frac{\partial}{\partial t} \{\mathcal{H}(\mathbf{r}, t) \exp[i(q_y y - \omega t)]\}, \\ \nabla \times \mathcal{H}(\mathbf{r}, t) \exp[i(q_y y - \omega t)] \\ &= \epsilon_0 \frac{\partial}{\partial t} \{\epsilon(y, t) \mathcal{E}(\mathbf{r}, t) \exp[i(q_y y - \omega t)]\}, \end{aligned} \quad (\text{A1})$$

where  $\epsilon_0$  is the electric permittivity of vacuum.

The periodic spatiotemporal variation of the permittivity tensor results in correspondingly periodic Floquet envelope functions, and thus, Maxwell equations can be solved by expanding these quantities in appropriate (truncated) Fourier series. Considering solutions in the form of plane waves in the  $x$ - $z$  plane where the medium is homogeneous, we have

$$\begin{aligned} \epsilon(\mathbf{r}, t) &= \sum_{n=-N}^N \epsilon(n) \exp[-in(SQy - \Omega t)], \\ \mathcal{E}(\mathbf{r}, t) &= E_0 \sum_{n=-N}^N \mathbf{e}(n) \exp[i(q_x x + q_z z)] \\ &\quad \times \exp[-in(SQy - \Omega t)], \quad (\text{A2}) \\ \mathcal{H}(\mathbf{r}, t) &= \frac{E_0}{Z_0} \sum_{n=-N}^N \mathbf{h}(n) \exp[i(q_x x + q_z z)] \\ &\quad \times \exp[-in(SQy - \Omega t)], \end{aligned}$$

where  $Z_0$  is the impedance of free space,  $\mathbf{e}$  and  $\mathbf{h}$  are polarization vectors chosen such that  $\sum_{n=-N}^N \mathbf{e}(n) \cdot \mathbf{e}^*(n) = 1$ , and

$E_0$  defines the field amplitude. Substituting Eqs. (A2) into Eqs. (A1), we obtain

$$\begin{aligned} \mathbf{q}_n \times \mathbf{h}(n) + k_n \sum_{n'=-N}^N \epsilon(n-n') \mathbf{e}(n') &= 0, \\ \mathbf{q}_n \times \mathbf{e}(n) - k_n \mu \mathbf{h}(n) &= 0 \end{aligned} \quad (\text{A3})$$

for  $n = -N, -N+1, \dots, N$ , with  $\mathbf{q}_n = (q_x, q_y - nSQ, q_z)$  and  $k_n = (\omega - n\Omega)/c$ , where  $c = 1/\sqrt{\epsilon_0\mu_0}$  is the speed of light in vacuum. Equation (A3) can be cast in the form of a  $6(2N+1) \times 6(2N+1)$  linear eigenvalue problem,

$$\begin{pmatrix} \underline{\underline{\mathbf{k}}}\underline{\underline{\epsilon}} & \underline{\underline{\mathbf{C}}}\underline{\underline{\mu}} \\ -\underline{\underline{\mathbf{C}}}\underline{\underline{\mu}} & \underline{\underline{\mathbf{k}}}\underline{\underline{\mu}} \end{pmatrix}^{-1} \begin{pmatrix} \underline{\underline{\mathbf{0}}} & \underline{\underline{\mathbf{D}}} \\ -\underline{\underline{\mathbf{D}}} & \underline{\underline{\mathbf{0}}} \end{pmatrix} \begin{pmatrix} \underline{\underline{\mathbf{e}}} \\ \underline{\underline{\mathbf{h}}} \end{pmatrix} = \frac{1}{q_z} \begin{pmatrix} \underline{\underline{\mathbf{e}}} \\ \underline{\underline{\mathbf{h}}} \end{pmatrix}, \quad (\text{A4})$$

which can be solved by standard numerical algorithms [58]. In Eq. (A4), by a double underscore we denote  $3(2N+1) \times 3(2N+1)$  matrices;  $\underline{\underline{\mathbf{0}}}$  is the zero matrix, and  $\underline{\underline{\mathbf{k}}} = \text{diag}(\mathbf{k}_{-N}, \mathbf{k}_{-N+1}, \dots, \mathbf{k}_N)$ , with  $\mathbf{k}_n = \mathbf{I}k_n$  and  $\mathbf{I}$  being the  $3 \times 3$  unit matrix.  $\underline{\underline{\mathbf{C}}} = \text{diag}(\mathbf{C}_{-N}, \mathbf{C}_{-N+1}, \dots, \mathbf{C}_N)$  and  $\underline{\underline{\mathbf{D}}} = \text{diag}(\mathbf{D}, \mathbf{D}, \dots, \mathbf{D})$  are block diagonal matrices, with

$$\begin{aligned} \mathbf{C}_n &= \begin{pmatrix} 0 & 0 & q_y - nSQ \\ 0 & 0 & -q_x \\ -q_y + nSQ & q_x & 0 \end{pmatrix}, \\ \mathbf{D} &= \begin{pmatrix} 0 & 1 & 0 \\ -1 & 0 & 0 \\ 0 & 0 & 0 \end{pmatrix}, \end{aligned} \quad (\text{A5})$$

while  $\underline{\underline{\epsilon}}$  is the Toeplitz matrix of the Fourier coefficients of the electric permittivity tensor

$$\underline{\underline{\epsilon}} = \begin{pmatrix} \epsilon(0) & \epsilon(-1) & \dots & \epsilon(-2N) \\ \epsilon(1) & \epsilon(0) & \dots & \epsilon(-2N+1) \\ \vdots & \vdots & \ddots & \vdots \\ \epsilon(2N) & \epsilon(2N-1) & \dots & \epsilon(0) \end{pmatrix}. \quad (\text{A6})$$

Correspondingly,  $\underline{\underline{\mathbf{e}}}$  and  $\underline{\underline{\mathbf{h}}}$  are  $3(2N+1)$ -dimensional vectors,

$$\underline{\underline{\mathbf{e}}} = \begin{pmatrix} \mathbf{e}(-N) \\ \mathbf{e}(-N+1) \\ \vdots \\ \mathbf{e}(N) \end{pmatrix}, \quad \underline{\underline{\mathbf{h}}} = \begin{pmatrix} \mathbf{h}(-N) \\ \mathbf{h}(-N+1) \\ \vdots \\ \mathbf{h}(N) \end{pmatrix}. \quad (\text{A7})$$

The  $4(2N+1)$  physically acceptable solutions, corresponding to the nonzero eigenvalues of Eq. (A4), are characterized by a superscript  $s = +(-)$ , which denotes waves propagating or decaying in the positive (negative)  $z$  direction, a subscript  $p = 1, 2$  indicating the two eigenpolarizations, and another subscript,  $v = -N, -N+1, \dots, N$ , that labels the different eigenmodes. The electric and magnetic field components of these modes with eigenvalues  $q_{pvz}^s$  and polarization eigenvectors  $\mathbf{e}_{pv}^s(n)$  and  $\mathbf{h}_{pv}^s(n)$ , assuming unit amplitude, according to Eq. (A2), are given by

$$\begin{aligned} \mathcal{E}_{pv}^s(\mathbf{r}, t) &= \sum_{n=-N}^N \exp[i(q_x x + q_{pvz}^s z)] \\ &\times \exp[-in(SQy - \Omega t)] \mathbf{e}_{pv}^s(n), \end{aligned}$$

$$\begin{aligned} \mathcal{H}_{pv}^s(\mathbf{r}, t) &= \frac{1}{Z_0} \sum_{n=-N}^N \exp[i(q_x x + q_{pvz}^s z)] \\ &\times \exp[-in(SQy - \Omega t)] \mathbf{h}_{pv}^s(n). \end{aligned} \quad (\text{A8})$$

In the case of static homogeneous media, Eq. (A4) is reduced to a set of  $2N+1$  independent eigenvalue equations [59],

$$\begin{pmatrix} k_n \epsilon & \mathbf{C}_n \\ -\mathbf{C}_n & k_n \mu \mathbf{I} \end{pmatrix}^{-1} \begin{pmatrix} \mathbf{0} & \mathbf{D} \\ -\mathbf{D} & \mathbf{0} \end{pmatrix} \begin{pmatrix} \mathbf{e} \\ \mathbf{h} \end{pmatrix} = \frac{1}{q_z} \begin{pmatrix} \mathbf{e} \\ \mathbf{h} \end{pmatrix}, \quad (\text{A9})$$

one for each value of  $n = -N, -N+1, \dots, N$ , where  $\epsilon$  are the elements of the corresponding static dielectric tensor. From the physically acceptable eigenvectors  $\mathbf{e}_{pn}^s$  and  $\mathbf{h}_{pn}^s$  of Eqs. (A9), we construct the eigenvectors which appear in Eqs. (A8), setting  $\mathbf{e}_{pv}^s(n) = \delta_{vn} \mathbf{e}_{pn}^s$  and  $\mathbf{h}_{pv}^s(n) = \delta_{vn} \mathbf{h}_{pn}^s$ , while the corresponding wave vectors are  $\mathbf{q}_{pv}^s = \mathbf{q}_{pn}^s$ .

Scattering at a planar  $x$ - $y$  interface between two different, in general spatiotemporal periodic, media can be described in the same manner as in Ref. [44] for corresponding time-varying media, the only difference being that, here, the common periodicity of both media on either side of the interface implies that not only the Floquet quasifrequency  $\omega$  but also the Floquet quasiwavenumber  $q_y$  remains invariant. Imposing continuity of the tangential components of the EM field at the interface yields the appropriate transmission and reflection matrices. The transmission and reflection matrices of such a stratified medium are obtained by properly combining those of its successive interfaces to take into account all multiple-scattering processes. In the present work, we are concerned with a multilayer slab comprising spatiotemporal periodic media, bounded by two semi-infinite homogeneous and isotropic static media: A on its left and B on its right, characterized by scalar relative electric permittivities  $\epsilon_A, \epsilon_B$  and magnetic permeabilities  $\mu_A, \mu_B$ , respectively. The transmittance and reflectance of this slab, for a light beam of order  $n'$  and polarization  $p'$  incident from the left, are given by

$$\mathcal{T} = \sum_{p,n} \mathcal{T}_{pn} = \sum_{p,n} |Q_{pn;p'n'}^I|^2 \frac{\text{Re}[q_{nz}^{+(B)}] \mu_A}{\text{Re}[q_{n'z}^{+(A)}] \mu_B}, \quad (\text{A10})$$

$$\mathcal{R} = \sum_{p,n} \mathcal{R}_{pn} = \sum_{p,n} |Q_{pn;p'n'}^{III}|^2 \frac{\text{Re}[q_{nz}^{-(A)}]}{\text{Re}[q_{n'z}^{+(A)}]}, \quad (\text{A11})$$

where  $q_{nz}^{\pm(m)} = \pm \sqrt{k_n^2 \epsilon_m \mu_m - q_x^2 - (q_y - nSQ)^2}$ , with  $m = A, B$  denoting the appropriate medium.  $Q_{pn;p'n'}^I$  and  $Q_{pn;p'n'}^{III}$  are the elements of the transmission and reflection matrices of the slab, respectively, for incidence from the left. Because of the time variation of the permittivity tensor, the EM energy is not conserved even in the absence of dissipative (thermal) losses. In this case,  $\mathcal{A} = 1 - \mathcal{T} - \mathcal{R} > 0 (< 0)$  means energy transfer from (to) the EM to (from) the spin-wave field.

It should be pointed out that the formalism developed here goes beyond the linear-response approximation, which is usually employed in Brillouin light scattering studies [56,60] (in fact, our method is correct to any order in perturbation theory), and the quasistatic adiabatic approach [40,42,43]. It is a rigorous, fully dynamic theory, which is able to describe, among other things, the interaction of strongly modulated



light as it propagates through a judiciously designed photonic structure with spin waves when both fields are concurrently localized in the same region of space (optomagnonic cavity).

In this respect, it is also not restricted to strongly reflecting surfaces [56,60] or waveguide geometries [7–11] considered in previous inelastic-light-scattering studies.

- 
- [1] R. W. Damon and J. R. Eshbach, *J. Phys. Chem. Solids* **19**, 308 (1961).
- [2] P. Grunberg and F. Metawe, *Phys. Rev. Lett.* **39**, 1561 (1977).
- [3] B. Hillebrands, P. Baumgart, and G. Guntherodt, *Phys. Rev. B* **36**, 2450 (1987).
- [4] G. Srinivasan, C. E. Patton, and P. R. Emtage, *J. Appl. Phys.* **61**, 2318 (1987).
- [5] A. A. Stashkevich, P. Djemia, Y. K. Fetisov, N. Bizière, and C. Fermon, *J. Appl. Phys.* **102**, 103905 (2007).
- [6] W. Bang, J. Lim, J. Trossman, D. Amanov, M. B. Jungfleisch, A. Hoffmann, and J. B. Ketterson, *J. Appl. Phys.* **123**, 123902 (2018).
- [7] A. D. Fisher, J. N. Lee, E. S. Gaynor, and A. B. Tveten, *Appl. Phys. Lett.* **41**, 779 (1982).
- [8] R. Bhandari and Y. Miyazaki, *Jpn. J. Appl. Phys.* **23**, 171 (1984).
- [9] A. D. Fisher, *Circuits Syst. Signal Process.* **4**, 265 (1985).
- [10] C. S. Tsai, D. Young, W. Chen, L. Adkins, C. C. Lee, and H. Glass, *Appl. Phys. Lett.* **47**, 651 (1985).
- [11] A. Prabhakar and D. Stancil, *IEEE Trans. Magn.* **32**, 1918 (1996).
- [12] H. Tamada, M. Kaneko, and T. Okamoto, *J. Appl. Phys.* **64**, 554 (1988).
- [13] K. Hasegawa and Y. Miyazaki, *Jpn. J. Appl. Phys.* **29**, 270 (1990).
- [14] V. V. Matyushev, A. A. Stashkevich, and J. M. Desvignes, *J. Appl. Phys.* **69**, 5972 (1991).
- [15] D. Stancil, *IEEE J. Quantum Electron.* **27**, 61 (1991).
- [16] K. Hasegawa and Y. Miyazaki, *Jpn. J. Appl. Phys.* **30**, 188 (1991).
- [17] R. Bhandari and Y. Miyazaki, *IEICE Trans. Electron.* **E83-C**, 255 (2000).
- [18] A. Noguchi, N. Goto, and Y. Miyazaki, *Electr. Eng. Jpn.* **162**, 40 (2008).
- [19] D. Young and C. S. Tsai, *Appl. Phys. Lett.* **53**, 1696 (1988).
- [20] C. S. Tsai and D. Young, *Appl. Phys. Lett.* **54**, 196 (1989).
- [21] N. Bilaniuk, D. D. Stancil, and S. H. Talisa, *J. Appl. Phys.* **67**, 508 (1990).
- [22] V. V. Matyushev, M. P. Kostylev, A. A. Stashkevich, and J. M. Desvignes, *J. Appl. Phys.* **77**, 2087 (1995).
- [23] A. D. Boardman, Y. V. Gulyaev, and S. A. Nikitov, *Jpn. J. Appl. Phys.* **27**, L2438 (1988).
- [24] C. S. Tsai, Y. S. Lin, J. Su, and S. R. Calciu, *Appl. Phys. Lett.* **71**, 3715 (1997).
- [25] Y. K. Fetisov and A. A. Klimov, *J. Opt. Soc. Am. B* **22**, 274 (2005).
- [26] Y. Tabuchi, S. Ishino, A. Noguchi, T. Ishikawa, R. Yamazaki, K. Usami, and Y. Nakamura, *Science* **349**, 405 (2015).
- [27] D. Lachance-Quirion, Y. Tabuchi, S. Ishino, A. Noguchi, T. Ishikawa, R. Yamazaki, and Y. Nakamura, *Sci. Adv.* **3**, e1603150 (2017).
- [28] T. Liu, X. Zhang, H. X. Tang, and M. E. Flatté, *Phys. Rev. B* **94**, 060405(R) (2016).
- [29] S. Viola Kusminskiy, H. X. Tang, and F. Marquardt, *Phys. Rev. A* **94**, 033821 (2016).
- [30] S. Sharma, Y. M. Blanter, and G. E. W. Bauer, *Phys. Rev. Lett.* **121**, 087205 (2018).
- [31] V. A. S. V. Bittencourt, V. Feulner, and S. V. Kusminskiy, *Phys. Rev. A* **100**, 013810 (2019).
- [32] A. Osada, R. Hisatomi, A. Noguchi, Y. Tabuchi, R. Yamazaki, K. Usami, M. Sadgrove, R. Yalla, M. Nomura, and Y. Nakamura, *Phys. Rev. Lett.* **116**, 223601 (2016).
- [33] X. Zhang, N. Zhu, C.-L. Zou, and H. X. Tang, *Phys. Rev. Lett.* **117**, 123605 (2016).
- [34] J. A. Haigh, A. Nunnenkamp, A. J. Ramsay, and A. J. Ferguson, *Phys. Rev. Lett.* **117**, 133602 (2016).
- [35] S. Sharma, Y. M. Blanter, and G. E. W. Bauer, *Phys. Rev. B* **96**, 094412 (2017).
- [36] A. Osada, A. Gloppe, R. Hisatomi, A. Noguchi, R. Yamazaki, M. Nomura, Y. Nakamura, and K. Usami, *Phys. Rev. Lett.* **120**, 133602 (2018).
- [37] A. Osada, A. Gloppe, Y. Nakamura, and K. Usami, *New J. Phys.* **20**, 103018 (2018).
- [38] J. A. Haigh, N. J. Lambert, S. Sharma, Y. M. Blanter, G. E. W. Bauer, and A. J. Ramsay, *Phys. Rev. B* **97**, 214423 (2018).
- [39] S. Sharma, B. Z. Rameshti, Y. M. Blanter, and G. E. W. Bauer, *Phys. Rev. B* **99**, 214423 (2019).
- [40] E. Almpanis, *Phys. Rev. B* **97**, 184406 (2018).
- [41] J. Graf, H. Pfeifer, F. Marquardt, and S. Viola Kusminskiy, *Phys. Rev. B* **98**, 241406(R) (2018).
- [42] P. A. Pantazopoulos, N. Stefanou, E. Almpanis, and N. Papanikolaou, *Phys. Rev. B* **96**, 104425 (2017).
- [43] P.-A. Pantazopoulos, N. Papanikolaou, and N. Stefanou, *J. Opt.* **21**, 015603 (2018).
- [44] P. A. Pantazopoulos and N. Stefanou, *Phys. Rev. B* **99**, 144415 (2019).
- [45] P. A. Pantazopoulos, K. L. Tsakmakidis, E. Almpanis, G. P. Zouros, and N. Stefanou, *New J. Phys.* **21**, 095001 (2019).
- [46] M. Kostylev and A. A. Stashkevich, *J. Magn. Magn. Mater.* **484**, 329 (2019).
- [47] D. L. Sounas and A. Alù, *Nat. Photonics* **11**, 774 (2017).
- [48] T. T. Koutserimpas, A. Alu, and R. Fleury, *Phys. Rev. A* **97**, 013839 (2018).
- [49] K. Giergiel, A. Dauphin, M. Lewenstein, J. Zakrzewski, and K. Sacha, *New J. Phys.* **21**, 052003 (2019).
- [50] A. M. Shaltout, V. M. Shalaev, and M. L. Brongersma, *Science* **364**, eaat3100 (2019).
- [51] M. C. Onbasli, L. Beran, M. Zahradník, M. Kučera, R. Antoš, J. Mistrík, G. F. Dionne, M. Veis, and C. A. Ross, *Sci. Rep.* **6**, 23640 (2016).
- [52] D. T. Pierce and W. E. Spicer, *Phys. Rev. B* **5**, 3017 (1972).
- [53] L. Gao, F. Lemarchand, and M. Lequime, *Opt. Express* **20**, 15734 (2012).

- [54] D. D. Stancil and A. Prabhakar, *Spin Waves: Theory and Applications* (Springer, Boston, 2009).
- [55] R. E. De Wames and T. Wolfram, *J. Appl. Phys.* **41**, 987 (1970).
- [56] R. E. Camley, T. S. Rahman, and D. L. Mills, *Phys. Rev. B* **27**, 261 (1983).
- [57] M. Aspelmeyer, T. J. Kippenberg, and F. Marquardt, *Rev. Mod. Phys.* **86**, 1391 (2014).
- [58] W. H. Press, S. A. Teukolsky, W. T. Vetterling, and B. P. Flannery, *Numerical Recipes Edition: The Art of Scientific Computing*, 3rd ed. (Cambridge University Press, Cambridge, 2007).
- [59] A. Christofi and N. Stefanou, *Phys. Rev. B* **97**, 125129 (2018).
- [60] R. E. Camley, T. S. Rahman, and D. L. Mills, *Phys. Rev. B* **23**, 1226 (1981).